An automated colorimetric inline titration of CO_2 concentrations in solvent flow streams using a Teflon AF-2400 tube-in-tube device.

Matthew O'Brien*

Lennard-Jones Laboratories, School of Chemical and Physical Sciences, Keele University, Borough of Newcastle-under-Lyme, Staffordshire, United Kingdom of Great Britain and Northern Ireland, ST5 5BG.

Abstract

Using a number of open source software components (Python, SciPy, OpenCV, PySerial), together with an inexpensive webcam device, an automated inline colorimetric titration methodology was developed to measure CO_2 concentration levels in organic flow streams emerging from a Teflon AF-2400 tube-in-tube device. A bisection search algorithm was used in combination with a curve-fitting approach to determine colorimetric titration endpoints. The results obtained are consistent with a simple 'negative exponential' model of permeation/dissolution.

Introduction

Carbon dioxide is the principle carbon-containing by-product from fossil fuel combustion. It is also released in significant quantities as a result of other industrial processes, including the production of cements from limestone. According to a recent 2016 report,[1] the gas is currently being released into the atmosphere at a rate of approximately 36.2 billion tonnes per annum. Despite growing momentum towards alternative energy sources (nuclear, solar, wind, hydroelectric etc.), as of 2014 fossil fuels still accounted for around 81% of all energy production worldwide.[2] As CO_2 has been implicated as a major causative factor in anthropogenic post-industrial climate change, its generation and release continues to pose a significant environmental threat.[3]

In addition to the increased adoption of low carbon energy sources, carbon-capture-and-storage (CCS)[4] and carbon dioxide utilisation (CDU also known as carbon capture and utilisation – CCU)[5-7] have been identified as potential strategies for the mitigation of industrial carbon dioxide release. As CO_2 has value as a C-1 building block in the chemical synthesis of a number of useful materials,[8-15] CDU represents an attractive approach that offers both environmental and economic benefits.

Although CO_2 undergoes many reactions in the gas-phase, for the majority of reactions with liquid or solid reaction partners it will be necessary to use a solvent. Indeed, it is generally the case in chemical synthesis that solvent plays a significant role in determining the outcome and/or efficiency of the desired transformation.[16] In order to obtain optimal reaction stoichiometries and kinetic parameters for any particular solvent, it will clearly be important to gain control over the concentration of CO_2 in that solvent.

We have previously shown[17] that continuous flow gas-liquid reactors based on the semi-permeable Teflon AF-2400[18-20] fluoropolymer facilitate the efficient, reliable and controllable generation of homogenous flow streams of reactive gasses in organic solvents. In addition to providing a high degree of control over gas concentration levels, continuous flow approaches to

organic synthesis readily lend themselves to the idea of direct utilisation of carbon dioxide at the point of production, as the gas is being generated.

Whilst remaining impermeable to the liquid phase, Teflon AF-2400 allows gasses to rapidly permeate through its amorphous microporous structure.[21, 22] Initially used in synthetic applications with ozone,[23] these devices have since been used with a diverse array of gasses including hydrogen,[24, 25] ammonia,[26-28] oxygen,[29-34] ethene,[35-37] carbon monoxide,[38, 39] syngas[40] and diazomethane[41, 42]. Jensen and co-workers have also used this material to remove an ethene by-product in a continuous flow application.[43] Importantly, in the context of this present work we, and others, have demonstrated their use with carbon dioxide as a gaseous reaction partner.[44, 45] Additionally, Teflon AF-2400 has been used in a number CO_2 sensing applications, particularly in the context of environmental research.[46-48]

In applications where pressurised gas is required to achieve the desired solution concentration, the simple 'tube-in-tube' configuration allows an inner Teflon AF-2400 tube to be surrounded by a relatively thin jacket of pressurised gas contained in a non-permeable outer tube (Figure 1, which shows the diameters of the tube-in-tube device used in this work). This requires only a small volume of gas to be pressurised at any time, thus minimising any hazard in the event of a rupture.

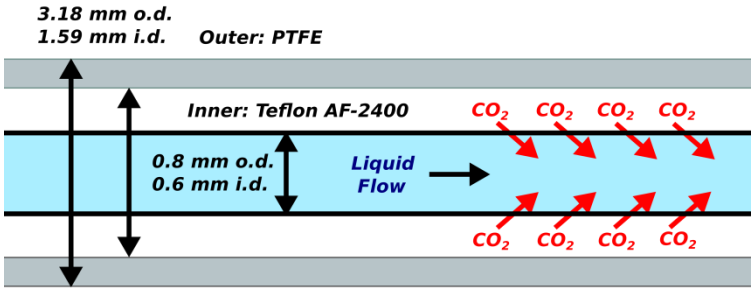

Figure 1. Basic schematic of the Tube-in-Tube device. The liquid flowing through the inner Teflon AF-2400 tubing is represented by the blue colour. The device used in this work had a length of 10 cm.

These devices potentially offer certain advantages over mechanical approaches to continuous flow gas-liquid contacting. In systems where gas and liquid flow streams meet at a mixing junction and form a biphasic outlet stream, control over the interfacial surface area, which depends on the exact morphology of the mixing junction, is by no means trivial and a number of interesting engineering approaches to this problem have been developed.[49-51] By providing an alternative mechanism for gas-liquid contact, membrane devices directly generate homogeneous flow streams of gas in liquid, circumventing many of these issues.

Jensen and co-workers have performed detailed computational studies on the membrane permeation in these tube-in-tube devices which predict relatively straightforward behaviour following standard permeation-diffusion models.[52] This is in line with our previous findings using

hydrogen in dichloromethane,[24] where very rapid saturation was obtained (within a few seconds) and where saturation concentrations were proportional to pressure, in accordance with Henry's law.[53]

We have utilised a number of methods for the determination of gas concentrations in solutions generated using these tube-in-tube devices. In the hydrogen study mentioned above we developed a novel 'bubble counting' technique to quantify the out-gassing of dissolved hydrogen downstream of the back-pressure regulator. This gave results which were in agreement with standard burette measurements of out-gassing. A burette was also used to measure the out-gassing of dissolved oxygen.[30] With carbon monoxide, in-line FTIR analysis provided a convenient method of gas quantification.[39] For ammonia, its basic reactivity was utilised in an in-line colorimetric acid-base titration.[26] Very recently, the Jensen group have reported an efficient automated approach, using mass flow metering, for the determination of gas take-up by solvents in tube-in-tube devices.[54]

In this manuscript we report the development of an automated inline colorimetric titration of CO_2 concentrations in acetonitrile flow streams generated using a Teflon AF-2400 tube-in-tube device. Incorporating a number of open-source software components (OpenCV,[55, 56] Python,[57] SciPy[58, 59], PySerial[60]) in combination with an inexpensive webcam device, the methodology described builds on our previous research in this area[61-66] and uses a computer-vision approach[67] to determine the colorimetric endpoint.

Due to the acidity of CO_2, concentrations of the gas can be determined using a colorimetric titration against a known concentration of a basic species. For this work, an aqueous sodium hydroxide solution was used in conjunction with a phenolphthalein indicator (which exists in an intensely coloured purple dianonic form at pH values above about 8.2[68]).

In the titration reaction, one equivalent of hydroxide reacts with aqueous CO_2 (which exists in equilibrium with the hydrated carbonic acid form H_2CO_3) to form the bicarbonate anion HCO_3^-. Excess hydroxide deprotonates the bicarbonate anion to form carbonate, CO_3^{2-}. The apparent pKa$_1$ value for carbonic acid,[68-70] which combines the equilibrium constant for the $(H_2O + CO_2)/H_2CO_3$ reaction with the acid dissociation constant for H_2CO_3 is 6.35 (Figure 2).

$$CO_2 + H_2O \rightleftharpoons H_2CO_3$$

$$H_2CO_3 + OH^- \rightleftharpoons HCO_3^- + H_2O$$

$$pK_{a1}(app) = 6.35$$

$$HCO_3^- + OH^- \rightleftharpoons CO_3^{2-} + H_2O$$

$$pK_{a2} = 10.33$$

Figure 2. Relevant equilibria in the acid-base reactivity of aqueous CO_2.

The p*K*a value for bicarbonate, HCO_3^-, is 10.33. As such, the lower pH value for the visibility range of phenolphthalein, 8.2, will be close to the point of maximum gradient in the intermediate region of the titration curve, making it an excellent indicator for this purpose. This is illustrated in Figure 3.

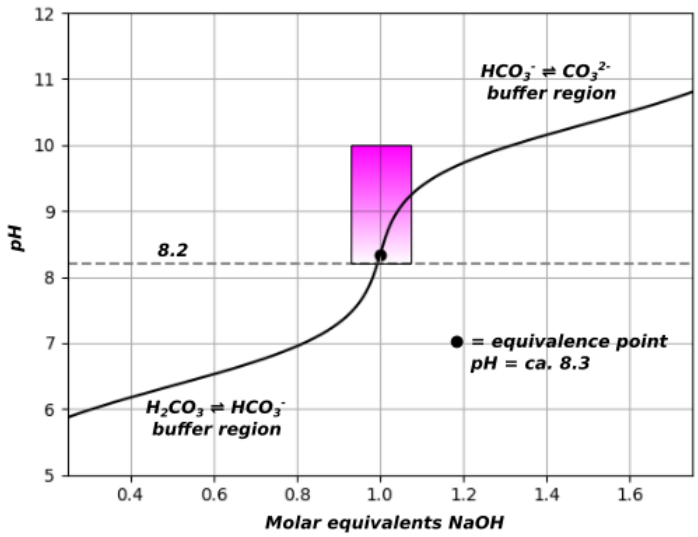

Figure 3. The lower pH visibility limit of phenolphthalein colouration (purple box) superimposed on a calculated titration curve for aqueous CO_2, showing the overlap with the equivalence point. The titration curve was calculated using pHcalc[71], a Python library for the systematic calculation of solution pH values[72].

Results and Discussion

The general setup for the apparatus is shown in Figure 4. Acetonitrile is pumped from a reservoir through a tube-in-tube device with an inner 10 cm length of Teflon AF-2400 (corresponding to a fixed volume of 0.028 mL). The outer containing tube is connected, via a pressure regulator, to a CO_2 cyclinder. The residence time of the acetonitrile in the tube-in-tube device is determined by the flow rate. The CO_2 enriched acetonitrile that exits the tube-in-tube device meets a stream of 0.06 M aqueous sodium hydroxide solution (which contains phenolphthalein at a concentration of 0.64 mM) at the t-piece. The combined flow stream then passes through an active inline mixer to disrupt any laminar flow and ensure thorough mixing of the two solutions. This inline mixer consists of several small PTFE coated magnetic stirrer bars contained within a narrow glass omnifit column placed on the plate of a magnetic stirrer-hotplate (see images provided in the Supporting Information). The action of the rotating magnetic field causes the constrained stirrer bars to precess rapidly around an average longitudinal axis, facilitating rapid mixing. The mixed solution then passes through a length of translucent tubing coiled around a white cylinder. This is enclosed, along with a diffuse LED light source and a webcam device, within a light-proof chamber to prevent any interference from variation in ambient light levels. The webcam is connected to the control computer which also controls the flow rate of the sodium hydroxide titrant solution through an RS232/serial connection.

The 11 bar (gauge) back pressure regulator prevents the upstream out-gassing of dissolved CO_2, ensuring homogeneity of the solution.

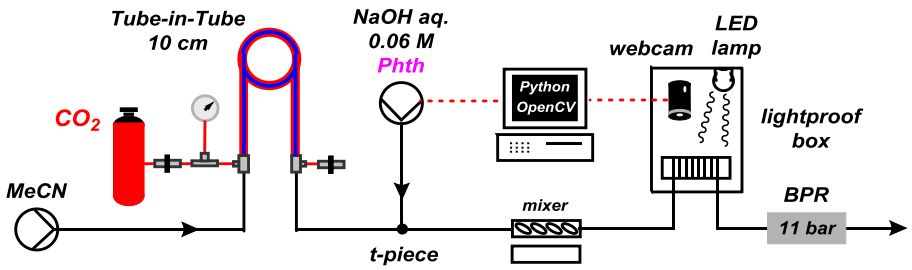

Figure 4. Apparatus setup for inline titrations. BPR = back pressure regulator. Phth = Phenolphthalein.

The general principle of the in line titration is straightforward. For a particular combination of acetonitrile flow rate and CO_2 pressure, the amount of CO_2 exiting the tube-in-tube reactor per unit time is determined by finding the flow rate of the sodium hydroxide titrant required to just reach the colorimetric endpoint observed via the webcam. At this point the molar flow rate of sodium hydroxide is taken as equal to the molar flow rate of CO_2. The concentration of CO_2 in acetonitrile is then calculated by dividing the molar flow rate of CO_2 by the flow rate of acetonitrile.

In order to determine the colorimetric endpoint in an automated manner, it is necessary to have a well-defined metric for colour intensity. The approach adopted in this work treats the [R, G, B] pixel colour values from the webcam as analogous to vectors.[61, 73] From the webcam, the colour of the solution passing through a defined section of the coiled tubing downstream of the mixer is obtained as the [R, G, B] triple averaged over that section of the image. Prior to the start of the pumping sequence, a 'zero-intensity' calibration [R, G, B] triple is obtained for solution with no phenolphthalein indicator. Likewise, a 'full-intensity' calibration [R, G, B] triple is obtained for the phenolphthalein/NaOH solution alone. The [R, G, B] calibration 'vector', $\boldsymbol{c}$, for the phenolphthalein solution itself is then given by the difference between the [R, G, B] triples for the 'full-intensity' and 'zero-intensity' calibration solutions. The [R, G, B] 'vector', $\boldsymbol{m}$, of the solution being quantified at any particular time is then the [R, G, B] triple measured at that time minus the [R, G, B] triple of the 'zero-intensity' calibration solution. The proportional 'scalar projection', $\boldsymbol{p}$, of the measured 'vector', $\boldsymbol{m}$, on the calibration 'vector', $\boldsymbol{c}$, is then calculated[74] as an indicator of colour intensity between these values:

$$\boldsymbol{p} = \boldsymbol{m} \cdot \frac{\boldsymbol{c}}{|\boldsymbol{c}|} = \frac{\boldsymbol{m}^T \boldsymbol{c}}{\boldsymbol{c}^T \boldsymbol{c}}$$

(where $\boldsymbol{m}^T$ is the transpose of $\boldsymbol{m}$).

Calculated projection values then range from 0 (for a solution with no purple colour) to 1 (for a solution with the same purple colour as the phenolphthalein/NaOH titrant solution alone). This is illustrated in Figure 5.

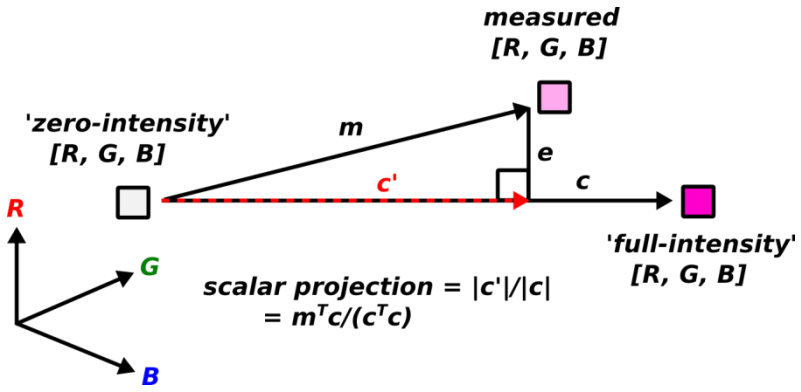

Figure 5. Scalar projection |**c'**|/|**c**| of measured [R, G, B] 'vector' ***m*** onto 'full intensity' vector ***c***.

Although the [R, G, B] colour space is clearly not a linear vector space (ranging from [0,0,0] for absolute darkness to [255,255,255] for the intensity of light which just saturates the three colour channels), this method nevertheless provides a robust measure of colour intensity.

In addition to the reduction in colour intensity due to the reaction of any CO_2 present with the sodium hydroxide in the titrant solution, the intensity will also be reduced as the result of simple dilution in the absence of CO_2. Shown in Figure 6 is a graph showing how the colour intensity (calculated as the scalar projection, ***p***) at two fixed flow rates of acetonitrile (0.8 mL min^{-1} and 1.2 mL min^{-1}) varied with the flow rate of the titrant solution. In this case, the Tube-in-Tube device was bypassed to prevent the introduction of CO_2. The python script used to control the titrant pump and to connect to the webcam and calculate colour intensity is provided in the Supporting Information files. Measurements were made for 20 titrant flow rates, equally spaced over a range from 0.5 mL min^{-1} to 5 mL min^{-1}. For each flow rate, 15 measurements of colour intensity were made, 5 seconds apart. The first 7 measurements (corresponding to 35 seconds) for each flow rate were ignored. This time was determined to be sufficient to allow solution to pass through the mixing device and to achieve a new 'steady state' for each titrant speed. The average values, taken from the following 8 measurements for each flow rate is indicated by the large red coloured circles. The time series data points are shown with smaller pink circles. In practice the titrant flow speeds were ramped downwards from 5.0 mL min^{-1} to 0.5 mL min^{-1}. The time between each data point, and the time between each flow rate was the same throughout the run, so the 5.0 – 0.5 mL min^{-1} flow rate range corresponds to a time range between 0 and 1500 seconds. For the range of titrant flow rates investigated, the colour intensity displays a reasonably linear response to the flow rate of the titrant solution in both cases. As the colour intensity will tend towards an asymptotic maximum (of 1.0) at higher titrant flow rates, any data fitting function must behave likewise. From a range of candidate functions, the hyperbolic tangent function, ***tanh***, was found to provide an excellent single-parameter fit to the obtained data. Shown in Figure 6 are the least-squares curves of best fit for ***tanh(f/m)***, (where ***f*** is the flow rate and ***m*** is a single parameter representative of the curve), along with the corresponding coefficients of determination (R^2 values). These curves were fitted using the

optimize.curve_fit tool in SciPy (trust region reflective algorithm). The ratio of the ***m*** parameter for the two curves, 1.46, is in good agreement with the ratio (1.5) of the fixed acetonitrile flow rates, consistent with the conservation of colour intensities for mixtures of equal acetonitrile/titrant composition. The ***m*** parameter can be seen as a rescaling parameter for the horizontal flow axis with differing acetonitrile speeds.

It should be pointed out that any mathematical fitting functions used in this work, whilst providing a good fit to the calculated colour intensity data, are in no way intended to model the concentration of any chemical species in solution. The purpose of finding suitable fitting functions is merely to provide a better estimate of the horizontal intercept of the colour intensity curve in the inline titrations. Importantly, it is clear from Figure 6 that the colour intensity curves will intercept the horizontal axis at or very close to zero, indicating that zero colour intensity in the absence of CO_2 can only be achieved when there is zero concentration of the indicator in its coloured form. In other words, for all positive concentrations of titrant/indicator, the annihilation of colour intensity (i.e. at the apparent colorimetric endpoint) can only be achieved through reaction with CO_2 and not merely through dilution effects.

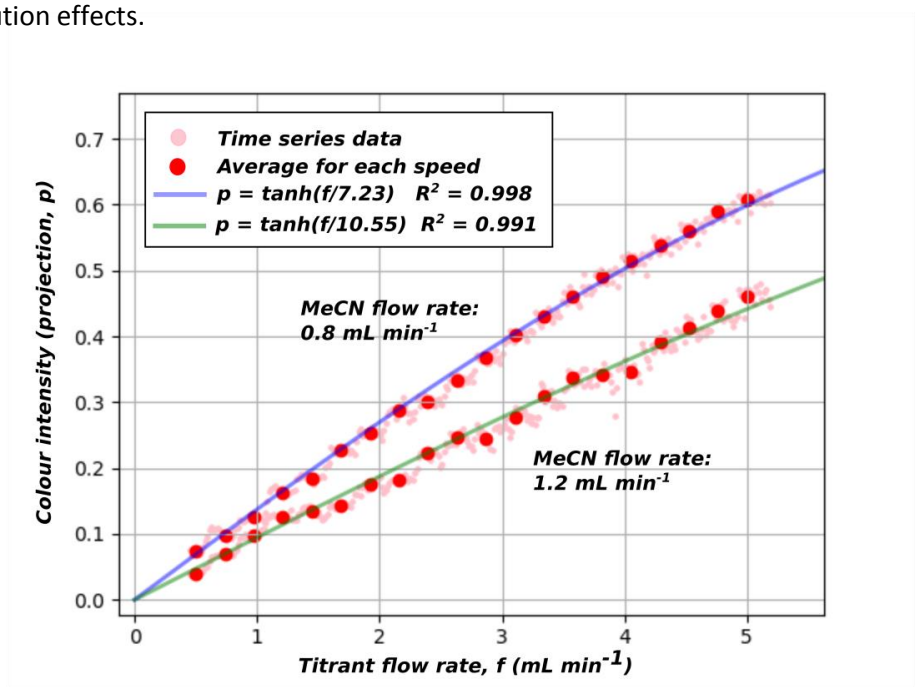

Figure 6. Response of colour intensity to titrant flow rate in the absence of CO_2, at two different flow rates of acetonitrile.

In order to test the general validity of the colorimetric titration methodology prior to working with CO_2 itself, experiments were carried out with known concentrations of acetic acid in acetonitrile. The graphs of colour intensity against titrant flow rate for solutions of acetic acid in acetonitrile (at 0.076, 0.151 and 0.227 M concentrations) flowing at 0.8 mL min^{-1} are shown in Figure 7, together with the previously obtained curve for acetonitrile alone at this flow rate. As with the previous experiment, several measurements were made at each titrant flow rate and the average value (shown in blue) was taken. The time between each measurement, and the time between each flow rate step was the same throughout. In each case, at high titrant flow rates, the curve coincides with the dilution curve obtained using acetonitrile alone. At a particular titrant flow rate there is a very sharp drop in the

colour intensity (to zero) as the flow rate of the titrant drops below that required to maintain alkalinity. This was taken to be the colorimetric endpoint. Using a colour intensity of 0.05 as a threshold, the highest titrant flow rate giving a colour intensity less than this was taken as an approximate lower bound for the colorimetric endpoint. Likewise, the lowest titrant flow rate giving a colour intensity higher than this was taken as the upper bound for the colorimetric endpoint.

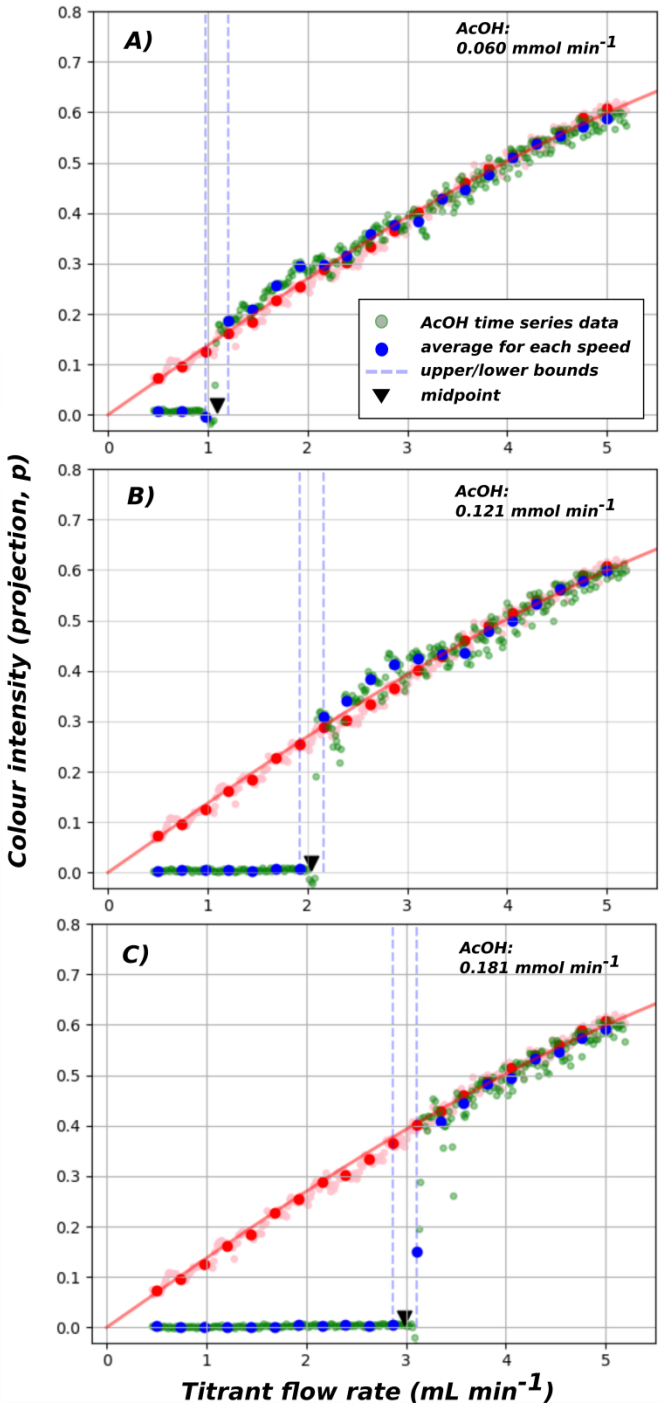

Figure 7. Colorimetric titrations of known concentrations of acetic acid (0.076, 0.151, 0.227 M) in acetonitrile at a flow rate of 0.8 mL min^{-1}. The previously obtained 'dilution' curve for colour intensity is shown in red/pink.

Using these values, a plot of the molar flow rate of acetic acid against the molar flow rate of titrant at the endpoint is shown in Figure 8. There is a good fit to a straight line passing through the origin with a slope very close to 1.0. For each molar AcOH flow rate, the actual matching titrant flow rate is between the upper and lower titrant estimates derived from the colorimetric webcam experiment (Table 1), indicating general agreement between calculated and actual acetic acid concentrations (the blue upper/lower bounds in Figure 8 correspond to the blue dashed lines in Figure 7).

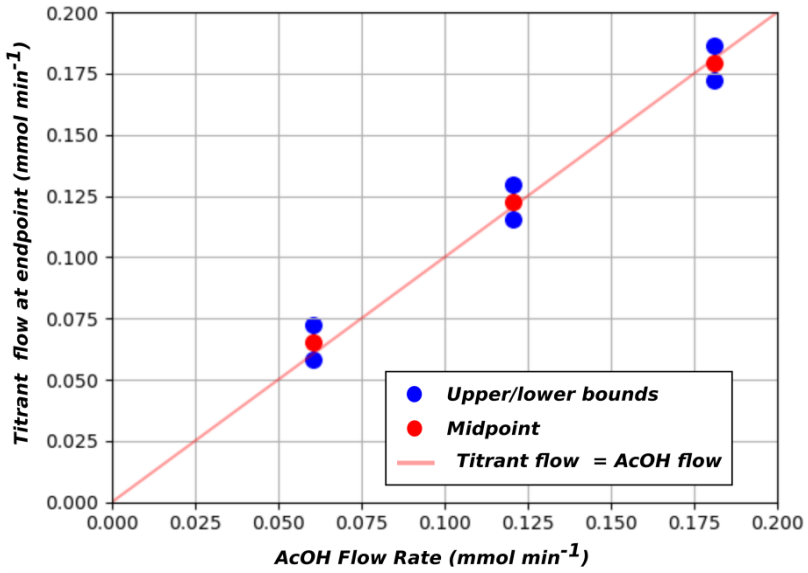

Figure 8. Plot of endpoint titrant flow rates against the molar flow rates of acetic acid. The blue upper/lower bounds correspond to the dashed blue lines in Figure 7. The red midpoint indicators correspond to the black midpoint indicators in Figure 7.

AcOH (mmol min^{-1})	**Titrant flow range (mmol min^{-1})**	**Titrant midpoint (mmol min^{-1})**
0.060	0.058 – 0.073	0.066
0.121	0.115 – 0.129	0.122
0.181	0.172 – 0.186	0.179

Table 1. AcOH molar flow rates and the estimated upper and lower titrant bounds from the webcam colorimetric experiment.

With the general validity of the colorimetric titration established, a similar experiment was carried out using the tube-in-tube device pressurised with CO_2. A graph of the colour intensity against titrant flow rate for an acetonitrile flow rate of 0.8 mL min^{-1} and a CO_2 pressure of 5 bar (gauge) is shown in Figure 9. The situation is broadly similar to that observed with acetic acid. At high titrant flow rates (> 4 mL min^{-1}) the colour intensity trace coincides with that for acetonitrile alone. Below 2 mL min^{-1},

the colour intensity is essentially annihilated, indicating the complete neutralisation of the hydroxide titrant. The endpoint with CO_2 is significantly less sharp than that observed with acetic acid. This is in line with actual pH titration curves for the two acids and is to be expected given the much closer pKa values for the relevant species involved in the carbonic acid equilibria (10.33 and 6.35), compared with those for acetic acid (14 and 4.76). A plot of the corresponding calculated titration curves is provided in the Supporting Information.

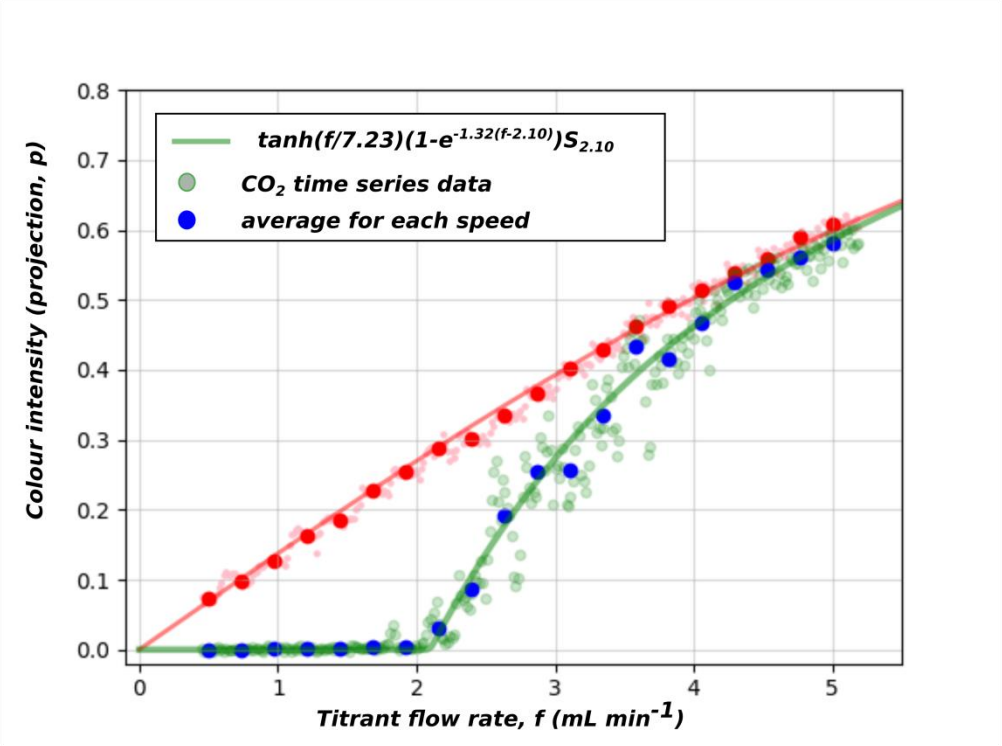

Figure 9. Colour intensity against titrant flow rate for a CO_2 pressure of 5 bar and an acetonitrile flow rate of 0.8 mL min^{-1}. The previously obtained 'dilution' curve for acetonitrile at 0.8 mL min^{-1} is shown in pink/red.

In the experiments carried out so far 20 titrant flow rates, equally spaced over the range from 0.5 mL min^{-1} to 5.0 mL min^{-1} were used. In order to more accurately determine the colorimetric endpoint, which was taken to be the exact point at which the colour intensity was reduced to zero, several approaches were considered. Whilst simply sampling at smaller intervals of titrant flow rate would by itself provide greater accuracy, this might significantly increase the amount of time taken to obtain results. In the context of obtaining CO_2 dissolution data for a wide range of different solvent systems, it might be desirable to develop more efficient methods. Another approach would be to fit the acquired data points to a suitable model, and then derive the horizontal intercept from the fitted parameters. A third option would be to use an iterative search approach to 'home in' on the intercept. As will be described, a methodology combining a bisection search algorithm and a curve-fitting approach facilitated efficient determination of colorimetric endpoints.

As the 'background' response of the colour intensity to simple dilution was found to be a close fit to the ***tanh(f/m)*** saturation function, the titration curve was considered to be a modulated form of this. The original ***m*** parameter of 7.23, which was previously fitted to the simple ***tanh(f/m)*** curve for the 0.8 mL min^{-1} acetonitrile dilution experiment was retained in subsequent curve fitting for this flow rate. For other acetonitrile flow rates, the ***m*** value used was scaled by a factor of ***r/0.8***, (where ***r*** is the acetonitrile flow rate) consistent with preserving constant colour intensity for dilutions of the same composition. Above the endpoint, the colour intensity curve rises from zero and approaches the 'background' ***tanh(f/m)*** dilution curve as a curvilinear asymptotic limit, suggestive of a simple shifted negative exponential curve in the form:

$$i = 1 - e^{-k(f-a)}$$

where ***f*** is the titrant flow rate and ***k*** and ***a*** are parameters. As the actual lower limit of the colour intensity is zero, a step function:

$$S_a = 1, \qquad f > a$$

$$S_a = 0, \qquad f \leq a$$

would provide the correct behaviour for flow rates below the endpoint. The overall function is the product of the ***tanh*** dilution function, the negative exponential function and the step function:

$$i = tanh\left(\frac{f}{m}\right) \cdot (1 - e^{-k(f-a)}) \cdot S_a$$

The required horizontal intercept value, ***a***, can then be read directly from the fitted parameters. The approach is illustrated graphically in Figure 10 which shows the three separate functions and the overall function which is their product.

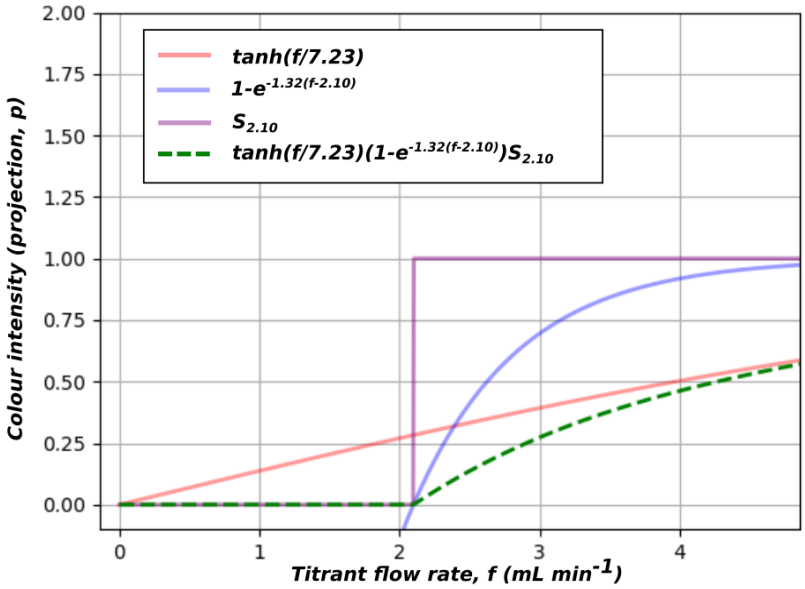

Figure 10. Modulating the fitted dilution function (***tanh***) with a negative exponential function and a step function provides an overall response function that provides a good fit to the observed colour intensity values (parameters shown were derived from curve fitting to the data shown in Figure 9).

As can be seen in Figure 9, the combined function for colour intensity (shown as a green line) provides a good fit to the experimental colour intensity data, with a coefficient of determination, R^2, of 0.995. Removing the data points for flow rates below the endpoint (which, being clamped at zero, do not provide any meaningful information and may artificially inflate the R^2 value) the R^2 value is still 0.987. The derived value for the horizontal intercept (the a parameter) is 2.10.

Having identified a suitable model function, a simple iterative bisection search method[75, 76] was adopted which would provide a greater number of data points close to the horizontal intercept.

The operation of the bisection method is as follows. Starting with an initial titrant flow rate, the colour intensity at this flow rate is obtained. If this is below a certain threshold value, the flow rate becomes the new minimum flow rate and the next flow rate tried is halfway between the current flow rate and the maximum flow rate. If the colour intensity is above the threshold, however, the flow rate becomes the new maximum flow rate and the next flow rate tried is halfway between the current flow rate and the minimum flow rate. This continues for the required number of iterations (or until convergence is reached).

Whilst the bisection method is capable of converging of providing very accurate convergence flow rates, it also susceptible to noise (one stray data point can lead to significant straying from the correct value). This is particularly true near the convergence point. By also using the curve-fitting approach with the colour intensity data collected during the bisection searches, a greater degree of reliability will be obtained. As all titrant flow rates below the colorimetric endpoints would provide colour intensities at or close to zero, zero itself would not be a suitable choice as a threshold for the algorithm converge on. Instead, a small but finite threshold of 0.05 was used. The python code for the algorithm is included in the Supporting Information files. For a particular combination of CO_2 pressure (either 5 bar or 10 bar (gauge)) and acetonitrile flow rate (between 0.2 and 3.6 mL min^{-1}), 4 bisection searches were run, each starting at a different titrant flow speed. This was done to ensure good coverage of the range of titrant flow rates (providing adequate data to fit curve parameters to) whilst also obtaining a greater proportion of data points nearer to the horizontal intercept. In each search, 9 iterations were run. As the error (the range between the minimum and maximum bounds) is halved for each iteration, in the absence of noise this would be sufficient to provide a titrant flow rate error of less than 0.009 mL min^{-1}, according to:

$$\varepsilon = \frac{\varepsilon^0}{2^n}$$

Where ε is the error obtained, ε^0 is the initial error (4.5 mL min^{-1} in this case, as the initial minimum and maximum values were 0.5 and 5.0 mL min^{-1}) and n is the number of iterations.

The flow rates and corresponding colour intensities for a single bisection run (with a starting flow rate of 1.5 mL min^{-1}) are shown in Figure 11. The acetonitrile flow rate was 0.6 ml min^{-1} and the CO_2 pressure was at 5 bar. The colour intensity for each iteration was the average of 60 measurements taken 1 second apart. A 30 second wait time, during which no measurements were taken, was included between each iteration to allow solution to clear the system. By definition of the bisection

algorithm, each flow rate lies between the two previous extrema. As can be seen, this was also true of the colour intensities, indicating proper convergence behaviour.

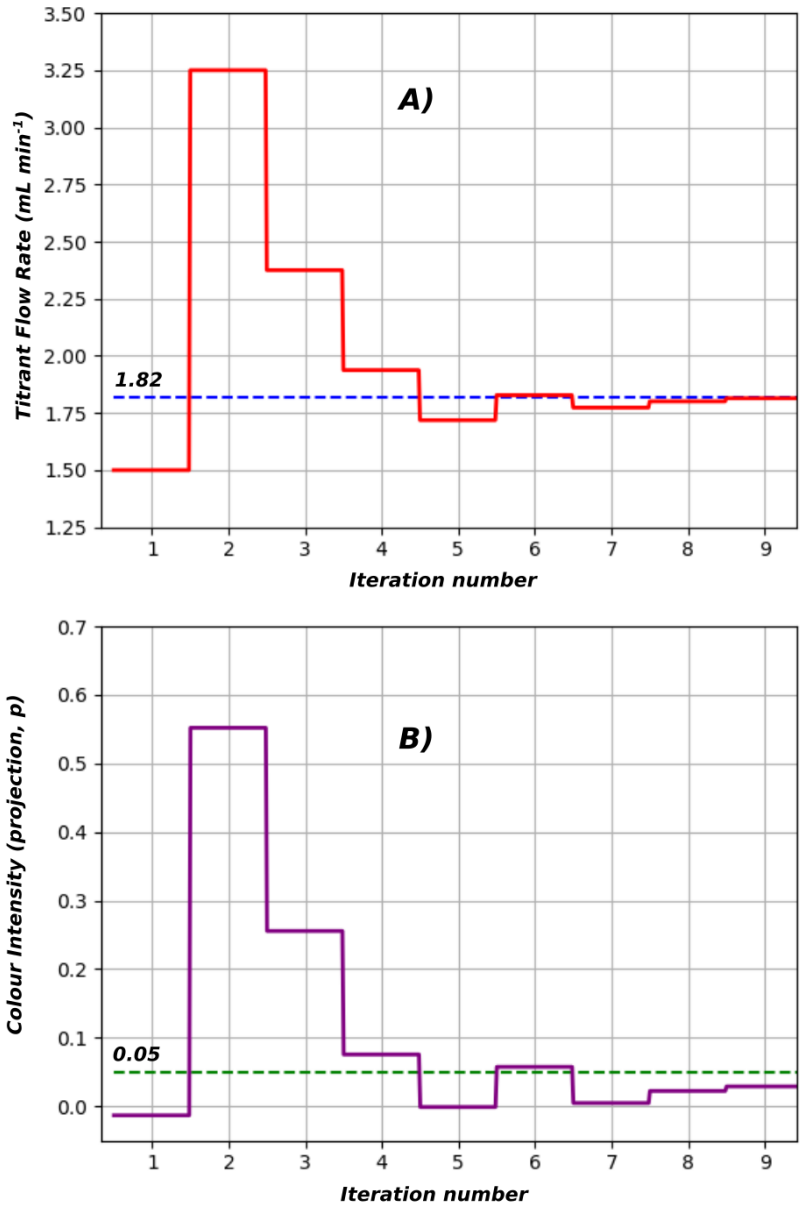

Figure 11. Plots of titrant flow rates (A) and average colour intensities (B) for each iteration of a bisection search with an initial flow rate of 1.5 mL min^{-1}. The colour intensity threshold of 0.05 is shown with a green dashed line in (B). The blue dashed line in (A) indicates the estimated convergence flow rate after 9 iterations.

Shown in Figure 12 are the data points obtained for all four iteration runs for this combination of acetonitrile flow rate and CO_2 pressure. The initial starting titrant flow speeds were 1.5, 2.5, 3.5, and 4.5 mL min^{-1} respectively. Data points for each set of iteration are shown in a different colour. The

curve of best fit for each set of iterations is shown in the same colour at the data points. An overall curve of best fit, fitted to the entire set of data points, is shown in black (which practically coincides with the curves for the 1.5 and 2.5 mL min^{-1} data sets). The final flow rate convergence value for each set of iterations is shown in yellow, on the 0.05 colour intensity line. As can be seen, there is very good agreement between these values. The average titrant flow rate over the four runs, based on these final data points, was 1.83 mL min^{-1}, with a standard deviation of 0.019 mL min^{-1}. The average calculated horizontal intercept for the fitted sets of curves was 1.746 mL min^{-1}, with a standard deviation of 0.014 mL min^{-1} and the horizontal intercept for the overall calculated curve was 1.745 mL min^{-1}. As expected, the titrant flow rate at the horizontal intercept (zero colour intensity) was slightly lower than that for a colour intensity threshold of 0.05.

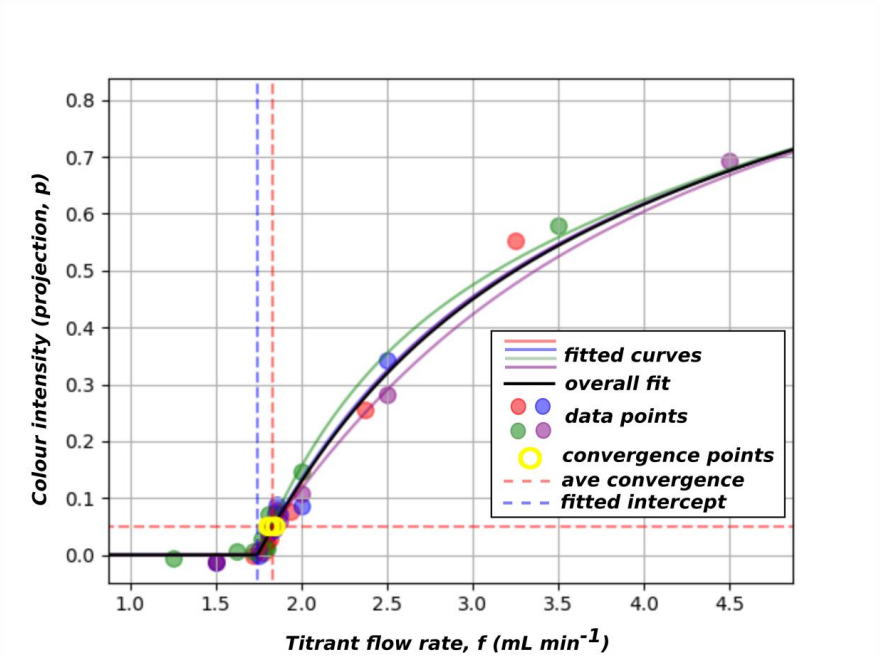

Figure 12. Data points and fitted curves from the bisection iteration experiment. CO_2 pressure was at 5 bar (gauge) and the acetonitrile flow rate was 0.6 mL min^{-1}. Each of the 4 sets of iterations was initiated at a different initial flow rate (Red: 1.5 ml min^{-1}, Blue: 2.5 mL min^{-1}, Green: 3.5 mL min^{-1}, Purple: 4.5 mL min^{-1}). The fitted curves for the Red and Blue data points are obscured by the black overall fitted curve (with which they practically coincide).

Using the same approach, a series of experimental runs were carried out for two CO_2 pressures, 5 and 10 bar (gauge), at a number of acetonitrile flow rates. The data for these, along with the fitted curves, are shown in Figure 13. The data points for each pressure/flow-rate combination are shown in different colours.

Each data set is the result 4 different bisection searches which commenced at different initial flow rates (1.5, 1.5, 3.5 and 4.5 mL min^{-1} for the 5 bar series, 1.5, 3.2, 4.9, 5.9 mL min^{-1} for the 10 bar series). The fitted curves for the 5 bar series are shown in orange, whilst the fitted curves for the 10 bar series are shown in green.

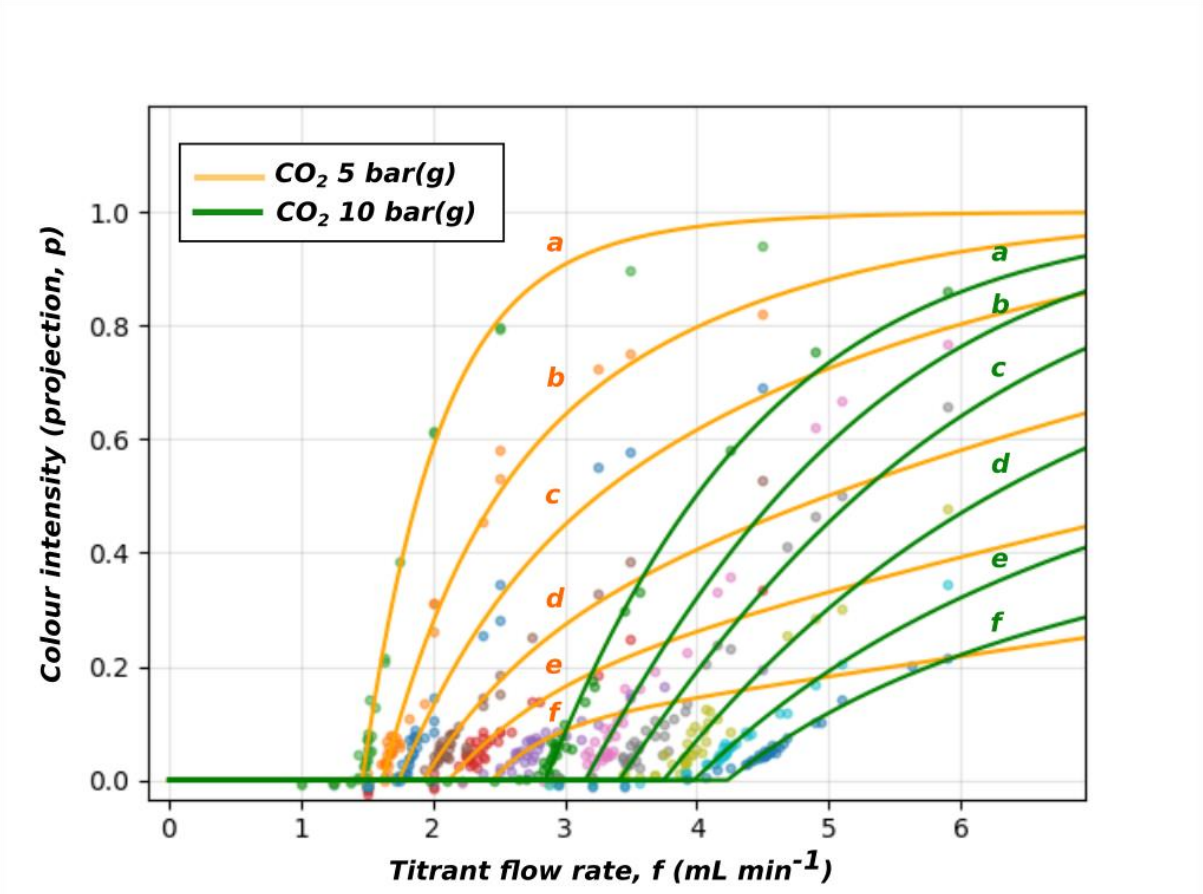

Figure 13. Colorimetric titration data and fitted curves for CO_2 at 5 bar gauge (orange, acetonitrile flow rates a-f = 0.2, 0.4, 0.6, 1.0, 1.6, 3.0 mL min^{-1}) and at 10 bar gauge (green, acetonitrile flow rates a-f = 0.2, 0.4, 0.6, 1.0, 1.6, 2.4 mL min^{-1}).

As the volume of the inner 10 cm tubing of the tube-in-tube device is 0.028 mL, the residence times correspond to this value divided by the acetonitrile flow rate. Shown in Figure 14 is a graph of the CO_2 concentrations derived from the colorimetric titrations plotted against the residence time. The data points from the bisection search using the 0.05 threshold of colour intensity are shown in blue, the data points using the calculated horizontal intercepts from the curve-fitting are shown in red. There is relatively little difference between the two sets.

For both pressures, the CO_2 concentration rises as the residence time increases and the gradient of the slope appears to reduce as the CO_2 concentration increases, presumably towards a saturation concentration at sufficiently high residence times.

Using a very simple model for the bulk concentration of CO_2 (ignoring any cross-section distribution within the tube), if the rate of change of the CO_2 concentration at any particular time is proportional to the difference between the current concentration and the maximum/saturation concentration, the following equation would apply:

$$\frac{dc}{dt} = k(S - c)$$

where c is concentration, S is the saturation concentration and k is a constant parameter.

This is easily solved by separation of variables to provide (assuming that $c = 0$ for $t = 0$) the following equation for c:

$$c = S(1 - e^{-kt})$$

This is in good agreement with the data obtained. The corresponding curve of best fit for each CO_2 pressure series (using the data points derived from the horizontal intercepts) is shown as a red line in Figure 14. The R^2 coefficient of determination was 0.996 for the 5 bar series and 0.998 for the 10 bar series.

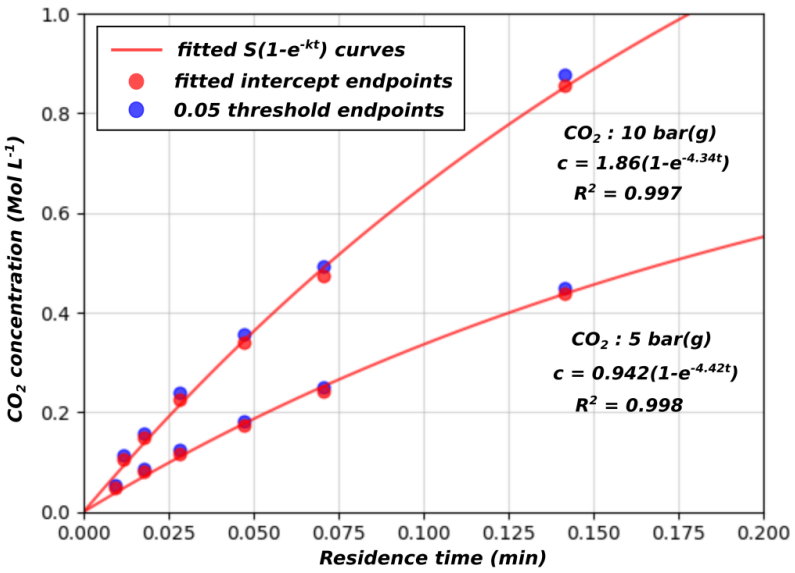

Figure 14. Plots of calculated CO_2 concentrations against residence time in the tube-in-tube device. Fitted curves (in red) are for the estimated horizontal intercepts. Residence time = (0.0283 mL)/(acetonitrile flow rate). CO_2 concentration = (titrant flow rate × titrant concentration)/(acetonitrile flow rate).

The ratio of the fitted saturation parameter, S, for the two curves (1.86 : 0.942 = 1.97 : 1.0) is in good approximate agreement with the ratio of the two absolute CO_2 pressures (11 : 6 = 1.83 : 1.0), in accordance with Henry's law. However, as the calculated concentrations obtained under these conditions are significantly lower than saturation concentrations, these values can only be treated as approximations.

Conclusion

The computer vision approach developed in this work provides a simple and inexpensive inline colorimetric titration for the determination of CO_2 concentrations in acetonitrile flow streams

generated using a Teflon AF-2400 tube-in-tube device. Using the [R, G, B] colourspace values as 'vector like' triples, a scalar projection furnishes a useful metric for colour intensity, facilitating automated methods for endpoint determination. An iterative bisection search algorithm was employed to converge on equivalent titrant flow speeds according to a set colour intensity threshold. A refined determination of colorimetric endpoints (corresponding to the complete annihilation of colour intensity) was effected using curve-fitting methodology on the data acquired from the bisection search process. The relationship between residence time (in the tube-in-tube device) and CO_2 concentration appears to follow a simple negative exponential equation, $\boldsymbol{c = S(1 - e^{-kt})}$. This is consistent with a simple permeation/dissolution model where the rate of change of concentration is proportional to the difference between the current concentration and the saturation concentration. In the context of CO_2 utilisation, particularly in synthetic chemistry applications, this highly predictable and inherently controllable behaviour imparted by the tube-in-tube device will facilitate precise control over reaction stoichiometries and kinetics, leading to efficient and scale-invariant transformations. We are currently using this inline colorimetric titration, in connection with tube-in-tube devices, to determine CO_2 concentrations in a range of organic flow streams and will report our findings in due course.

Experimental

Acetonitrile was purchased from Merck (LiChrosolv® Reag. Ph. Eur. grade). Carbon dioxide was purchased from BOC gasses. A GasArc Techmaster single stage regulator was used to regulate the CO_2 pressure. A Waters 600 pumping unit was used to deliver acetonitrile. Acetonitrile was delivered from a single pump channel. The remaining three pump channels, whilst not used, were primed with acetonitrile and attached to a full reservoir of the solvent. A Knauer Azura P 4.1S pump was used to deliver the titrant solution. A Newlink USB-0039DBL USB-to-RS232 adapter (purchased from CPC) was used to connect the control PC to the Knauer pump (via a crossover /'null modem' serial cable). The titrant was made from a freshly opened bottle of analytical grade sodium hydroxide (Fisher scientific). Phenolphthalein was purchased from Sigma-Aldrich. The titrant solution was stored and used under a positive pressure of nitrogen gas. Aside from the Tube-in-Tube device, FEP or PFA flow tubing was used (1.0 mm o.d 0.6 mm i.d.) and connected using Omnifit/Diba adapters and interconnects (1/4-28-UNF thread). The backpressure regulator was an Upchurch/IDEX type (Kinesis UK) and was manually adjusted to provide the desired back pressure of 11 bar (gauge), as measured using the pressure meter of the Knauer Azura pump. The webcam used was a Microsoft Lifecam-Cinema. All dynamic functions of the webcam (auto-white-balance, auto-focus, auto-exposure) were disabled and the same settings (shown in the Supplemental Information) were used for each run. The light used was a low-cost 4-LED diffused USB flexible reading light (XY-store/Amazon.co.uk) which was powered by a separate USB hub. Full details of the computer control and curve fitting processes (including Python source code) is provided in the Supporting Information. Further details and images of the Tube-in-Tube and inline mixing devices are provided in the Supporting Information.

Acknowledgements

We gratefully acknowledge funding from the UK EPSRC CO2Chem network (Seedcorn funding scheme). We are grateful to Dr Ilia Koev of Biogeneral Inc., San Diego, California, for donating the Teflon AF-2400 used in this work.

References

[1] J.G.J. Olivier;, G. Janssens-Maenhout;, M. Muntean;, J.A.H.W. Peters, Trends in global CO2 emissions: 2016 Report, Netherlands Environmental Assessment Agency, The Hague, 2016, PBL publication number: 2315, European Commission, Joint Research Centre, Science for Policy Report: 103428. http://edgar.jrc.ec.europa.eu/news_docs/jrc-2016-trends-in-global-co2-emissions-2016-report-103425.pdf (accessed August 2017).

[2] International Energy Agency; Key World Energy Statistics: 2016; https://www.iea.org/publications/freepublications/publication/KeyWorld2016.pdf (accessed August 2017).

[3] IPCC, 2014: Climate Change 2014: Synthesis Report. Contribution of Working Groups I, II and III to the Fifth Assessment Report of the Intergovernmental Panel on Climate Change [Core Writing Team, R.K. Pachauri and L.A. Meyer (eds.)]. IPCC, Geneva, Switzerland, 151 pp. https://www.ipcc.ch/report/ar5/syr/ (accessed August 2017).

[4] IPCC, 2005: IPCC Special Report on Carbon Dioxide Capture and Storage. Prepared by Working Group III of the Intergovernmental Panel on Climate Change [Metz, B., O. Davidson, H. C. de Coninck, M. Loos, and L. A. Meyer (eds.)]. Cambridge University Press, Cambridge, United Kingdom and New York, NY, USA, 442 pp.

[5] R.M. Cuellar-Franca, A. Azapagic, Carbon capture, storage and utilisation technologies: A critical analysis and comparison of their life cycle environmental impacts, J. CO2 Util. 9 (2015) 82-102.

[6] P. Markewitz, W. Kuckshinrichs, W. Leitner, J. Linssen, P. Zapp, R. Bongartz, A. Schreiber, T.E. Muller, Worldwide innovations in the development of carbon capture technologies and the utilization of CO2, Enegry Environ. Sci. 5(6) (2012) 7281-7305.

[7] A.J. Hunt, E.H.K. Sin, R. Marriott, J.H. Clark, Generation, Capture, and Utilization of Industrial Carbon Dioxide, ChemSusChem 3(3) (2010) 306-322.

[8] P. Styring, K. Armstrong, Catalytic carbon dioxide conversions to value-added chemicals, Chim. Oggi-Chem. Today 29(6) (2011) 34-37.

[9] A. Alissandratos, C.J. Easton, Biocatalysis for the application of CO2 as a chemical feedstock, Beilstein J. Org. Chem. 11 (2015) 2370-2387.

[10] A.-H. Liu, B. Yu, L.-N. He, Catalytic conversion of carbon dioxide to carboxylic acid derivatives, Greenhouse Gases-Science and Technology 5(1) (2015) 17-33.

[11] M. Taherimehr, P.P. Pescarmona, Green Polycarbonates Prepared by the Copolymerization of CO2 with Epoxides, J. App. Polym. Sci. 131(21) (2014).

[12] E.V. Kondratenko, G. Mul, J. Baltrusaitis, G.O. Larrazabal, J. Perez-Ramirez, Status and perspectives of CO2 conversion into fuels and chemicals by catalytic, photocatalytic and electrocatalytic processes, Enegry Environ. Sci. 6(11) (2013) 3112-3135.

[13] F. Manjolinho, M. Arndt, K. Gooßen, L.J. Gooßen, Catalytic C–H Carboxylation of Terminal Alkynes with Carbon Dioxide, ACS Catalysis 2(9) (2012) 2014-2021.

[14] M. North, R. Pasquale, C. Young, Synthesis of cyclic carbonates from epoxides and CO2, Green Chem. 12(9) (2010) 1514-1539.
[15] M. Aresta, A. Dibenedetto, Utilisation of CO2 as a chemical feedstock: opportunities and challenges, Dalton Trans. (28) (2007) 2975-2992.
[16] C. Reichardt, T. Welton, Eds., Solvents and Solvent Effects in Organic Chemistry, Wiley-VCH Verlag GmbH & Co. KGaA2010, pp. I-XXVI.
[17] M. Brzozowski, M. O'Brien, S.V. Ley, A. Polyzos, Flow Chemistry: Intelligent Processing of Gas-Liquid Transformations Using a Tube-in-Tube Reactor, Acc. Chem. Res. 48(2) (2015) 349-362.
[18] P.R. Resnick, US Patent 3978030

[19] P.R. Resnick, W.H. Buck, in Fluoropolymers II, eds. G. Hougham, P. E. Cassidy, K. Johns and T. Davidson, Kluwer Academic, New York, pp. 25-33 (1999).
[20] Biogeneral Inc., 9925 Mesa Rim Road, San Diego, California, USA. www.biogeneral.com (accessed August 2017).
[21] I. Pinnau, L.G. Toy, Gas and vapor transport properties of amorphous perfluorinated copolymer membranes based on 2,2-bistrifluoromethyl-4,5-difluoro-1,3-dioxole/tetrafluoroethylene, J. Membrane Sci. 109(1) (1996) 125-133.
[22] A.Y. Alentiev, Y.P. Yampolskii, V.P. Shantarovich, S.M. Nemser, N.A. Plate, High transport parameters and free volume of perfluorodioxole copolymers, J. Membrane Sci. 126(1) (1997) 123-132.
[23] M. O'Brien, I.R. Baxendale, S.V. Ley, Flow ozonolysis using a semipermeable Teflon AF-2400 membrane to effect gas-liquid contact, Org. Lett. 12(7) (2010) 1596-8.
[24] M. O'Brien, N. Taylor, A. Polyzos, I.R. Baxendale, S.V. Ley, Hydrogenation in flow: Homogeneous and heterogeneous catalysis using Teflon AF-2400 to effect gas-liquid contact at elevated pressure, Chem. Sci. 2(7) (2011) 1250-1257.
[25] S. Newton, S.V. Ley, E.C. Arce, D.M. Grainger, Asymmetric Homogeneous Hydrogenation in Flow using a Tube-in-Tube Reactor, Adv. Synth. Catal. 354(9) (2012) 1805-1812.
[26] D.L. Browne, M. O'Brien, P. Koos, P.B. Cranwell, A. Polyzos, S.V. Ley, Continuous-Flow Processing of Gaseous Ammonia Using a Teflon AF-2400 Tube-in-Tube Reactor: Synthesis of Thioureas and In-Line Titrations, Synlett (9) (2012) 1402-1406.
[27] P.B. Cranwell, M. O'Brien, D.L. Browne, P. Koos, A. Polyzos, M. Pena-Lopez, S.V. Ley, Flow synthesis using gaseous ammonia in a Teflon AF-2400 tube-in-tube reactor: Paal-Knorr pyrrole formation and gas concentration measurement by inline flow titration, Org. Biomol. Chem. 10(30) (2012) 5774-5779.
[28] J.C. Pastre, D.L. Browne, M. O'Brien, S.V. Ley, Scaling Up of Continuous Flow Processes with Gases Using a Tube-in-Tube Reactor: Inline Titrations and Fanetizole Synthesis with Ammonia, Org. Proc. Res. Dev. 17(9) (2013) 1183-1191.
[29] B. Tomaszewski, A. Schmid, K. Buehler, Biocatalytic Production of Catechols Using a High Pressure Tube-in-Tube Segmented Flow Microreactor, Org. Proc. Res. Dev. 18(11) (2014) 1516-1526.
[30] T.P. Petersen, A. Polyzos, M. O'Brien, T. Ulven, I.R. Baxendale, S.V. Ley, The Oxygen-Mediated Synthesis of 1,3-Butadiynes in Continuous Flow: Using Teflon AF-2400 to Effect Gas/Liquid Contact, ChemSusChem 5(2) (2012) 274-277.
[31] B. Tomaszewski, R.C. Lloyd, A.J. Warr, K. Buehler, A. Schmid, Regioselective Biocatalytic Aromatic Hydroxylation in a Gas-Liquid Multiphase Tube-in-Tube Reactor, ChemCatChem 6(9) (2014) 2567-2576.
[32] S.R. Chaudhuri, J. Hartwig, L. Kupracz, T. Kodanek, J. Wegner, A. Kirschning, Oxidations of Allylic and Benzylic Alcohols under Inductively-Heated Flow Conditions with Gold-Doped Superparamagnetic Nanostructured Particles as Catalyst and Oxygen as Oxidant, Adv. Synth. Catal. 356(17) (2014) 3530-3538.

[33] J.H. Park, C.Y. Park, M.J. Kim, M.U. Kim, Y.J. Kim, G.H. Kim, C.P. Park, Continuous-Flow Synthesis of meta-Substituted Phenol Derivatives, Org. Proc. Res. Dev. 19(7) (2015) 812-818.
[34] S. Sharma, R.A. Maurya, K.I. Min, G.Y. Jeong, D.P. Kim, Odorless Isocyanide Chemistry: An Integrated Microfluidic System for a Multistep Reaction Sequence, Angew. Chem.-Int. Edit. 52(29) (2013) 7564-7568.
[35] S.L. Bourne, P. Koos, M. O'Brien, B. Martin, B. Schenkel, I.R. Baxendale, S.V. Ley, The Continuous-Flow Synthesis of Styrenes Using Ethylene in a Palladium-Catalysed Heck Cross-Coupling Reaction, Synlett (18) (2011) 2643-2647.
[36] S.L. Bourne, M. O'Brien, S. Kasinathan, P. Koos, P. Tolstoy, D.X. Hu, R.W. Bates, B. Martin, B. Schenkel, S.V. Ley, Flow Chemistry Syntheses of Styrenes, Unsymmetrical Stilbenes and Branched Aldehydes, ChemCatChem 5(1) (2013) 159-172.
[37] C. Battilocchio, G. Iannucci, S. Wang, E. Godineau, A. Kolleth, A. De Mesmaeker, S.V. Ley, Flow synthesis of cyclobutanones via [2 + 2] cycloaddition of keteneiminium salts and ethylene gas, Reaction Chem. Eng. 2(3) (2017) 295-298.
[38] U. Gross, P. Koos, M. O'Brien, A. Polyzos, S.V. Ley, A General Continuous Flow Method for Palladium Catalysed Carbonylation Reactions Using Single and Multiple Tube-in-Tube Gas-Liquid Microreactors, Eur. J. Org. Chem. (29) (2014) 6418-6430.
[39] P. Koos, U. Gross, A. Polyzos, M. O'Brien, I. Baxendale, S.V. Ley, Teflon AF-2400 mediated gas-liquid contact in continuous flow methoxycarbonylations and in-line FTIR measurement of CO concentration, Org. Biomol. Chem. 9(20) (2011) 6903-6908.
[40] S. Kasinathan, S.L. Bourne, P. Tolstoy, P. Koos, M. O'Brien, R.W. Bates, I.R. Baxendale, S.V. Ley, Syngas-Mediated C-C Bond Formation in Flow: Selective Rhodium-Catalysed Hydroformylation of Styrenes, Synlett (18) (2011) 2648-2651.
[41] F. Mastronardi, B. Gutmann, C.O. Kappe, Continuous Flow Generation and Reactions of Anhydrous Diazomethane Using a Teflon AF-2400 Tube-in-Tube Reactor, Org. Lett. 15(21) (2013) 5590-5593.
[42] D. Dallinger, V.D. Pinho, B. Gutmann, C.O. Kappe, Laboratory-Scale Membrane Reactor for the Generation of Anhydrous Diazomethane, J. Org. Chem. 81(14) (2016) 5814-5823.
[43] E.J. O'Neal, K.F. Jensen, Continuous Nanofiltration and Recycle of a Metathesis Catalyst in a Microflow System, ChemCatChem 6(10) (2014) 3004-3011.
[44] A. Polyzos, M. O'Brien, T.P. Petersen, I.R. Baxendale, S.V. Ley, The Continuous-Flow Synthesis of Carboxylic Acids using CO2 in a Tube-In-Tube Gas Permeable Membrane Reactor, Angew. Chem.-Int. Edit. 50(5) (2011) 1190-1193.
[45] J.J.F. van Gool, S. van den Broek, R.M. Ripken, P.J. Nieuwland, K. Koch, F. Rutjes, Highly Controlled Gas/Liquid Processes in a Continuous Lab-Scale Device, Chem. Eng. Technol. 36(6) (2013) 1042-1046.
[46] P.L. Kebabian, A. Freedman, Fluoropolymer-based capacitive carbon dioxide sensor, Measurement Sci. Technol. 17(4) (2006) 703-710.
[47] R.R. Tiwari, Z.P. Smith, H.Q. Lin, B.D. Freeman, D.R. Paul, Gas permeation in thin films of "high free-volume" glassy perfluoropolymers: Part II. CO2 plasticization and sorption, Polymer 61 (2015) 1-14.
[48] Z.H.A. Wang, X.W. Liu, R.H. Byrne, R. Wanninkhof, R.E. Bernstein, E.A. Kaltenbacher, J. Patten, Simultaneous spectrophotometric flow-through measurements of pH, carbon dioxide fugacity, and total inorganic carbon in seawater, Anal. Chim. Acta 596(1) (2007) 23-36.
[49] N. Steinfeldt, R. Abdallah, U. Dingerdissen, K. JÃ¤hnisch, Ozonolysis of Acetic Acid 1-Vinyl-hexyl Ester in a Falling Film Microreactor, Org. Proc. Res. Dev. 11(6) (2007) 1025-1031.
[50] Y. Wada, M.A. Schmidt, K.F. Jensen, Flow Distribution and Ozonolysis in Gas−Liquid Multichannel Microreactors, Ind. Eng. Chem. Res. 45(24) (2006) 8036-8042.
[51] S. Hübner, U. Bentrup, U. Budde, K. Lovis, T. Dietrich, A. Freitag, L. Küpper, K. Jühnisch, An Ozonolysis-Reduction Sequence for the Synthesis of Pharmaceutical Intermediates in Microstructured Devices, Org. Proc. Res. Dev. 13(5) (2009) 952-960.

[52] L. Yang, K.F. Jensen, Mass Transport and Reactions in the Tube-in-Tube Reactor, Org. Proc. Res. Dev. 17(6) (2013) 927-933.
[53] W. Henry, Experiments on the Quantity of Gases Absorbed by Water, at Different Temperatures, and under Different Pressures, Phil. Trans. Royal Soc. London 93 (1803) 29-274.
[54] J. Zhang, A.R. Teixeira, H. Zhang, K.F. Jensen, Automated in Situ Measurement of Gas Solubility in Liquids with a Simple Tube-in-Tube Reactor, Anal. Chem. (2017).
[55] G. Bradski, The OpenCV library, Dr. Dobbs J. 25(11) (2000) 120-125.
[56] opencv.org/.
[57] G. van Rossum, Python tutorial, Technical Report CS-R9526, Centrum voor Wiskunde en Informatica (CWI), Amsterdam, May 1995. https://www.python.org/ (accessed August 2017).
[58] T.E. Oliphant, Python for scientific computing, Comp. Sci. Eng. 9(3) (2007) 10-20.
[59] Eric Jones, Travis Oliphant, P. Peterson, , SciPy: Open Source Scientific Tools for Python. http://www.scipy.org/, (accessed August 2017).
[60] https://github.com/pyserial/pyserial (accessed August 2017).
[61] M. O'Brien, P. Koos, D.L. Browne, S.V. Ley, A prototype continuous-flow liquid-liquid extraction system using open-source technology, Org. Biomol. Chem. 10(35) (2012) 7031-7036.
[62] D.X. Hu, M. O'Brien, S.V. Ley, Continuous Multiple Liquid–Liquid Separation: Diazotization of Amino Acids in Flow, Org. Lett. 14(16) (2012) 4246-4249.
[63] M. O'Brien, D.A. Cooper, J. Dolan, Continuous flow iodination using an automated computer-vision controlled liquid-liquid extraction system, Tetrahedron Letters 58(9) (2017) 829-834.
[64] M. O'Brien, D. Cooper, Continuous Flow Liquid-Liquid Separation Using a Computer-Vision Control System: The Bromination of Enaminones with N-Bromosuccinimide, Synlett 27(1) (2016) 164-168.
[65] M. O'Brien, D.A. Cooper, P. Mhembere, The continuous-flow synthesis of carbazate hydrazones using a simplified computer-vision controlled liquid-liquid extraction system, Tetrahedron Letters 57(47) (2016) 5188-5191.
[66] M. O'Brien, L. Konings, M. Martin, J. Heap, Harnessing open-source technology for low-cost automation in synthesis: Flow chemical deprotection of silyl ethers using a homemade autosampling system, Tetrahedron Letters 58(25) (2017) 2409-2413.
[67] S.V. Ley, R.J. Ingham, M. O'Brien, D.L. Browne, Camera-enabled techniques for organic synthesis, Beilstein J. Org. Chem. 9 (2013) 1051-1072.
[68] 'Handbook of chemistry and physics", 84th edition, edited by David R. Lide, CRC press, Boca Raton, Florida, US, 2003. .
[69] D.D. Perrin, Tables, Ionisation Constants of Inorganic Acids and Bases in Aqueous Solution (Second Edition), Pergamon1982, pp. 1-138.
[70] D. Pines, J. Ditkovich, T. Mukra, Y. Miller, P.M. Kiefer, S. Daschakraborty, J.T. Hynes, E. Pines, How Acidic Is Carbonic Acid?, J. Phys. Chem. B 120(9) (2016) 2440-2451.
[71] pHcalc; "Systemtic pH calculation package for Python"; Ryan Nelson; .https://pypi.python.org/pypi/pHcalc (accessed August 2017).
[72] J.J. Baeza-Baeza, M.C. García-Álvarez-Coque, Systematic Approach To Calculate the Concentration of Chemical Species in Multi-Equilibrium Problems, J. Chem. Educ. 88(2) (2011) 169-173.
[73] For a related approach to quantitative concentration determination using digital cameras, see: M.H.V. Werts, V. Raimbault, R. Texier-Picard, R. Poizat, O. Francais, L. Griscom, J.R.G. Navarro, Quantitative full-colour transmitted light microscopy and dyes for concentration mapping and measurement of diffusion coefficients in microfluidic architectures, Lab Chip 12(4) (2012) 808-820.
[74] Strang, Gilbert; "Linear Algebra and its Applications", 4th Edition, Brooks-Cole, Pacific Grove, CA, USA, 2006. .
[75] R. Burden, L., J.D. Faires, Numerical Analysis, 3rd Edition (2.1 The Bisection Algorithm), Prindle, Weber and Schmidt, Boston, MA, US, 1985.

[76] W. Cheney, D. Kincaid, Numerical Mathematics and Computing, Thomson Brooks/Cole, Belmont, CA, US, 2008.